Journal of Materials Chemistry C

Accepted Manuscript

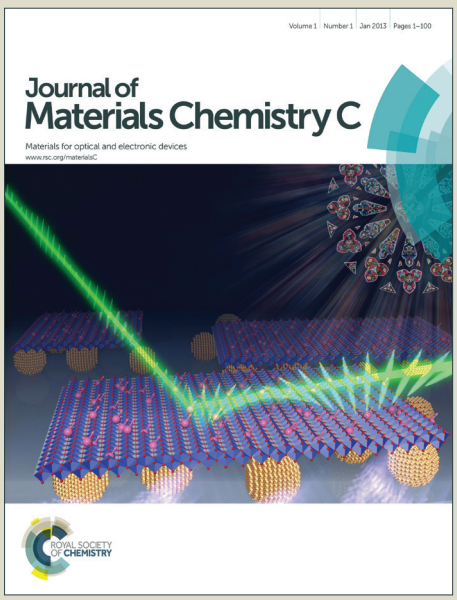

ROYAL SOCIETY OF CHEMISTRY

www.rsc.org/materialsC

Cite this: DOI: 10.1039/c0xx00000x

www.rsc.org/xxxxxx

ARTICLE TYPE

Influential effect of π-spacers, alkyl side chains, and of the various processing conditions on the photovoltaic properties of alkylselenyl substituted benzodithiophene based polymers

Kakaraparthi Kranthiraja,[‡a] Kumarasamy Gunasekar,[‡a] Woosum Cho,[a] Young Geun Park,[b] Jin Yong Lee,[b] Yurim Shin,[c] In-Nam Kang,[c] Myungkwan Song,[d] Keun Hwa Chae,[e] BongSoo Kim,[e] and Sung-Ho Jin*[a]

Received (in XXX, XXX) Xth XXXXXXXXX 20XX, Accepted Xth XXXXXXXXX 20XX

DOI: 10.1039/b000000x

π-Spacers and alkyl side chains play a key role in the optical, electrochemical, and photovoltaic properties of the π-conjugated polymers. To investigate the collective effect of π-spacers, alkyl side chains, and of the various processing conditions on the photovoltaic properties, an array of four new low band gap (LBG) π-conjugated polymers (**P1-P4**) were designed and synthesized for the application as donor materials in bulk heterojunction polymer solar cells (BHJ PSCs). These π-conjugated polymers contain benzodithiophene (BDT) donor unit substituted with 2-ethylhexylselenyl or 2-hexyldecylselenyl as π-conjugated side chains and dialkoxybenzothiadiazole (dialkoxyBT) electron deficient unit connected with thiophene or selenophene as π-spacers. Among four polymers, the absorption spectra of **P3** with thiophene π-spacer showed well enhanced vibronic shoulder peak between 620-650 nm, indicates **P3** possess strong interchain aggregation tendency and attain planar backbone structure due to the non-covalent interactions arise between sulfur atom in thiophene and oxygen atom in dialkoxyBT. Under suitable device processing conditions optimized pristine PSCs of **P3** showed maximum power conversion efficiency (PCE) of 4.09%. After employing 1,8-diiodooctane as an additive, one of the PSC devices based on **P2** displayed PCE of 5.34%. Though the active layers of **P1-P4** showed positive response towards methanol treatment, especially the **P3**-based devices delivered improved PCE of 5.63%, which was further assessed by electrical impedance spectroscopy. These findings in the current article provide good specimen for efficiently fine tuning the optical, photovoltaic properties of π-conjugated polymers via varying the size of alkyl chains, π-spacer groups and device processing conditions for the imminent growth of LBG π-conjugated polymers.

1. Introduction

In the last few years, excellent research on polymer-based organic photovoltaics (OPVs) has attracted special industrial and scientific interest.[1] A foremost enhancement in power conversion efficiency (PCE) has been accomplished via the use of bulk heterojunction (BHJ) architecture comprising an electron rich π-conjugated donor polymer and an electron accepting fullerene derivatives.[2] The intriguing device fabrication conditions, new device strategies and synthesis of new π-conjugated donor polymers have paved a smooth way to achieve PCE surpassing 10%.[3] The efficient donor polymers must have broad absorption for harvesting more solar flux, deep highest occupied molecular orbital (HOMO) energy level, and higher hole mobility.[4] Until now, the low band gap (LBG) donor polymers have been successfully synthesized by connecting the electron rich (D) and electron deficient (A) units in the polymer backbone. It is manifested that the D-A approach is highly efficient for regulating energy levels, carrier mobility, and reduce the bandgap energies of the polymers by prudent selection of D and A units.[5]

One of the best choices for designing highly efficient D-A based π-conjugated donor materials is to make use of π-spacers by locating them between the electron rich and deficient units. Generally, the introduction of π-spacers effectively reduces the steric hindrance between the D and A units, thus results in more planar structure for the polymer backbone.[6] Additionally, the π-spacers also plays a significant role in modulating the optical, electrochemical, and photovoltaic properties of the polymers.[7] Moreover, these bridging groups effectually brings the planarity to the polymer backbone using different non-covalent interactions that can exist between the heteroatom of π-spacers and donor or acceptor. 2,1,3-Benzothiadiazole (BT) is the most extensively used acceptor unit for constructing D-A polymers, which shown excellent photovoltaic properties.[8] Eventually, the bandgap of the corresponding polymers is reduced by adjusting their non-planar backbone conformation to planar structure.

Recently in D-A type polymers, different π-spacers including the aromatic rings varying from thiophene, selenophene, furan, and thieno[3,2-b]thiophene were introduced. Depending on the π-spacers moiety, variation of the optical, electrochemical, and photovoltaic properties were observed. For instance the replacement of thiophene with selenophene as a π-spacers is viewed as one of the best approaches for synthesizing π-conjugated polymers with narrow LBG in order to harvest more solar flux.[9] It is clearly understood that by just simply varying the π-spacers, it is possible to modulate the optical and electrochemical properties of the polymers, which in turn must have a significant effect on their photovoltaic properties. This motivated us to focus on seeking more information about the role of π-spacers in OPV research.

The photovoltaic properties of the π-conjugated polymers are not only dependent on the π-spacers but also on the type and position of solubilizing alkyl side chains attached to either electron rich or deficient part, since they can significantly affect the coplanarity, morphology, and photovoltaic parameters

of the polymers.[10] The fine architecture of alkyl side chains have to be addressed while designing new materials as these side chains play a crucial role in improving the molecular weight, solubility, and processability. Additionally, these alkyl chains can adjust intermolecular interactions and allow proper mixing with fullerene derivatives to form the desired morphology. Also, high priority should be given for the optimization of the alkyl side chain substituent's to attain equilibrium between short circuit current density (J_{sc}) and open-circuit voltage (V_{oc}) to realize maximum PCE.

It is fact that the nanoscale morphology of active layer is one of the key parameter, which influences the photovoltaic performance of BHJ PSC. In recent times, it was reported that among the various device engineering methods, PCE of PSCs can be significantly augmented by simple methanol treatment method prior to the deposition of the metal electrodes. Direct solvent exposure can influence the crystallanity, morphology, electrical characteristics of semiconductor.[11,12] A little amount of solvent that is added to the active layer will adjust the morphology in such a way to form nanoscale bicontinuous interpenetrating network.

In this scenario, we report the design and synthesis of an array of four D-A polymers, **P1-P4** comprising BDT with different side chain substituents (2-ethylhexylselenyl and 2-hexyldecylselenyl) and alternating dithienylbenzothiadiazole (DTBT) or diselenylbenzothiadiazole (DSeBT) repeating units in the polymer backbone. The combined effect of variation in the alkyl side chains and the π-spacer groups on the photovoltaic performance of the new BDTSe-based LBG polymers were investigated in detail. The difference in the π-spacers and length of side chains will have significant influence on the optical, morphological, and intrinsic photovoltaic properties of the polymers. Additionally, we employed external additives 1,8-diiodooctane (DIO), 1-chloronaphatlaene (CN) and polar solvent (methanol) treatment to obtain high PCE.

The BHJ PSCs of **P1-P4** showed significant improvement upon addition of DIO, along with methanol treatment also showed its own way of improving the PCE of **P1-P4**. Especially **P3**-based PSCs showed a PCE of 5.63% after treating the active layers with methanol. Herein, we paid our additional attention on study of enhanced PCE upon methanol treatment by electrical impedance spectroscopy, and found that device built in potential is increased by diminishing the amount of surface traps.

2. Experimental section

2.1. Materials

2-Hexyldecylbromide, 4,7-bis(5-bromothiophen-2-yl)-5,6-bis(octyloxy)benzo[*c*]thiadiazole (DTBT), and 4,7-bis(5-bromoselenophen-2-yl)-5,6-bis(octyloxy)benzo[*c*]thiadiazole (DSeBT) were synthesized according to the literature procedures [13,14]. Selenophene, n-BuLi, 2-ethylhexylbromide, trimethyltin chloride, tert-BuLi, tris(dibenzylideneacetone)palladium(0), and tri(o-tolyl)phosphine were purchased from Sigma-Aldrich Chemical Co. Ltd. The $PC_{71}BM$ was purchased from Solemme BV and the reagents and chemicals were purchased from Sigma-Aldrich Chemical Co. Ltd and TCI, which were used without further purification unless otherwise noted. Moisture sensitive reactions were conducted in the presence of N_2 atmosphere. The other materials were common chemical and used as received. THF was dried over Na/benzophenone ketyl and freshly distilled prior to use.

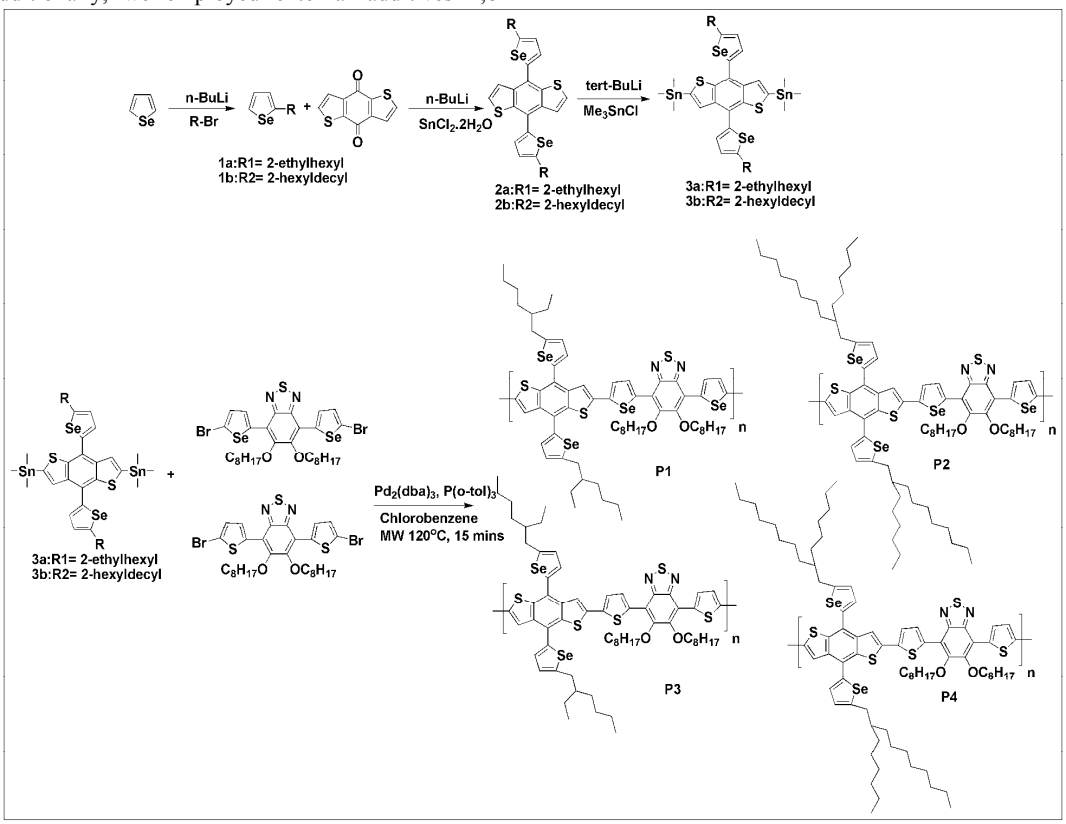

Scheme 1 Synthetic route for monomers and polymers.

2.2. Measurements

^{1}H and ^{13}C NMR spectra were recorded on a Varian Mercury Plus 300 MHz and 600 MHz spectrometer in $CDCl_3$ using tetramethylsilane as an internal reference. The chemical shifts were accounted in ppm related to the singlet of $CDCl_3$ at 7.26 and 77 ppm for ^{1}H and ^{13}C NMR, respectively. The UV-visible absorption spectra were recorded on a JASCO V-570 spectrophotometer. Polymerization was conducted in CEM focused microwave TM synthesis system (CEM Discover-S). The number average molecular weight (M_w) and polydispersity index (PDI) of the polymers were determined by gel permeation chromatography (GPC) using PL gel 5 µm MLXED-C column on an Agilent 1100 series liquid chromatography system with THF as an eluent and calibration with polystyrene standards. Thermal analysis was carried out on Mettler Toledo TGA/SDTA 851e, DSC 822e analyzer under N_2 atmosphere at heating rate of 10 ^{o}C/min. The cyclic voltammetry (CV) analyses were carried out with CHI 600C potentiostat (CH Instruments) at a scan rate of 100 mV/s in 0.1 M solution of tetrabutylammonium tetrafluoroborate in acetonitrile. A platinum wire was used as the counter electrode and an Ag/AgCl electrode was used as the reference electrode. X-ray diffraction measurements were carried out with Cu Kα (λ=1.54 Å) in a diffractometer (D8-ADVANCE, Bruker) equipped with Göbel mirror. The detector was scanned the angle (2Θ) from 0.1° to 35° with an incidence angle of 0.3°.

2.3. OTFT fabrication and characterization

OTFT devices were fabricated in a bottom contact geometry (channel length = 12 µm, width = 120 µm). The source and drain contacts consisted of gold (100 nm), and the dielectric was silicon oxide (SiO_2) with a thickness of 300 nm. The SiO_2 surface was cleaned, dried, and pretreated with a solution of octyltrichlorosilane (OTS-8, 1.0 mM) in toluene at room temperature for 2 h under N_2 to produce nonpolar and smooth surfaces onto which the polymers could be spin coated. The polymers were dissolved to a concentration of 0.5 wt% in chloroform. Films of the organic semiconductors were spin coated at 1500 rpm for 50 s to a thickness of 50 nm, followed by an annealing process (140 ^{o}C for 10 min under N_2 atmosphere). All device fabrication procedures and measurements were carried out in air at room temperature. The field effect mobility was calculated in the saturation regime by using the equation $I_{DS}=(\mu WC_i/2L)(V_G-V_T)^2$, where I_{DS} is the drain-source current, μ is the field effect mobility, W is the channel width (120 µm), L is the channel length (12 µm), C_i is the capacitance per unit area of the gate dielectric layer, and V_G is the gate voltage.

2.4. Fabrication and characterization of BHJ PSCs

The ITO coated glass substrates that have been used for fabrication were ultrasonically cleaned in detergent, water, acetone, and isopropyl alcohol. Then, a 35 nm thick layer of PEDOT:PSS (Clevios P VP AI 4083) was coated on the substrate. The coated buffer layer was cured at a temperature of 140 °C for 10 min in oven. Active layer was spin coated using a mixture of polymer:$PC_{71}BM$ that was dissolved in 1 mL of CB and further mixed with 1 vol% DIO for additive study. Whereas, methanol was spun coat on active layer at 2400 rpm for 40 s as post-deposition treatment. A 0.7 nm thickness of LiF and 100 nm thick Al cathode was deposited via evaporation on the active layer. The active area of the device was 0.09 cm^2. The thickness of the thin films was measured using a KLA Tencor Alpha-step IQ surface profilometer with an accuracy of ± 1 nm. AFM images were acquired using Park NX10 in tapping mode. The performance of PSCs were measured using a calibrated AM1.5G solar simulator (Oriel® Sol3A™ Class AAA solar simulator, models 94043A) with a light intensity of 100 mW/cm^2 adjusted using a standard PV reference cell (2 cm x 2 cm, mono crystalline silicon solar cell, calibrated at NREL, Colorado, USA) and a computer controlled Keithley 2400 source measure unit. Incident photon to current conversion efficiency (IPCE) spectrum was measured using Oriel® IQE-200™. While measuring the *J-V* curves for PSC, a black mask was used and only the effective area of the cell was exposed to light irradiation. The PSC device data's reported in this article, were confirmed for more than 5 iterations under the same condition.

2.5. Impedance spectroscopy

Impedance spectroscopy was measured with a VersaSTAT-3 (Princeton Applied Research) Workstation with an AC signal of 25 mV in the frequency range of 500 Hz to 1 MHz. Constant DC bias equivalent to open-circuit voltage of both pristine and methanol treated device was applied. Mott-schottky analysis was performed in the dark. The capacitance-voltage measurements were conducted at a frequency of 100 kHz and a AC bias of 25 mV. Mott-schottky analysis was performed in the dark. The capacitance-voltage measurements were conducted at a frequency of 100 kHz and a AC bias of 25 mV.

2.6. Hole and electron mobility

Hole-only and electron-only mobility measurement was performed using a device structure ITO/PEDOT:PSS/polymer (**P3**):$PC_{71}BM$/MoO_3/Al and of ITO/Al/**P3**:$PC_{71}BM$/Ca/Al. The mobility was determined by fitting the dark *J–V* curve into the space charge limited current (SCLC) model, based on the equation described by the Mott-Gurney law.

$J = (9/8)\varepsilon_r\varepsilon_0\mu(V^2/L^3)$

Where ε_r is the dielectric constant (ε_r=3), ε_0 is permittivity of free space, L the thickness of the active layer, µ is the charge mobility applied, and V is the voltage drop across the device.

2.7. Synthesis of monomers and polymers

2.7.1. Synthesis of 4,8-bis(5-ethylhexylselenophen-2-yl)benzo[1,2-b;4,5-b']dithiophene (2a). n-BuLi (2.5 M, 5.29 mL) was added dropwise to a solution of 2-ethylhexylselenophene (2.5 g, 9.87 mmol) in THF (50 mL) at 0 °C under N_2 atmosphere. The temperature of reaction mixture was raised to 50 °C and stirred for 1.5 h. 4,8-Dihydrobenzo[1,2-b:4,5- b']dithiophene-4,8-dione (0.52 g, 2.37 mmol) was added directly to the reaction mixture at 50 °C, which was then stirred for 2 h at the same temperature. Subsequently, the reaction mixture was cooled to room temperature and tin(II) chloride dihydrate (4.5 g, 19.75 mmol) in 15% HCl (20 mL) was added and further stirred for 1.5 h, which was poured into ice water. The reaction mixture was extracted with diethyl ether, the resultant organic layer was dried over anhydrous $MgSO_4$ and evaporated the solvent to get crude compound as brown oil. The crude was then purified by column chromatography on silica gel using hexane as an eluent to obtain 2a as yellow viscous oil (1.2 g, 72 %). ^{1}H NMR (300 MH_Z, $CDCl_3$): δ (ppm) 0.96 (m, 12H), 1.47–1.29 (m, 16H), 1.66 (m, 2H), 2.92 (d, 4H), 7.04 (d, 2H), 7.39 (d, 2H), 7.43 (d, 2H), 7.65 ppm (d, 1H). ^{13}C NMR (600 MH_Z, $CDCl_3$): δ (ppm) 11.12, 14.37, 23.23, 25.92, 29.15, 32.69, 32.70,

Table 1 Optical and electrochemical properties of **P1-P4**.

Polymer	Solution λ_{max} (nm)[a]	Film λ_{max} (nm)[b]	E_g^{opt} (eV)[c]	HOMO (eV)	LUMO (eV)
P1	614	610	1.69	-5.26	-3.57
P2	600	611	1.63	-5.40	-3.77
P3	589	589	1.76	-5.20	-3.44
P4	580	589	1.76	-5.22	-3.46

[a] Absorption maxima measured from UV-visible absorption spectrum in CF solution. [b] Absorption maxima measured from UV-visible absorption spectrum in thin film state. [c] Estimated from the onset of the absorption in thin films (E_g^{opt} = 1240/ λ_{onset}).

37.17, 37.21, 37.26, 42.44, 42.48, 123.72, 126.46, 130.22, 136.43, 138.99, 142.96, 154.07.

2.7.2. Synthesis of 2,6-bis(trimethyltin)-4,8-bis(5-ethylhexylselenophen-2-yl)benzo[1,2-b;4,5-b']dithiophene (2b). A solution of compound 2a (1.1 g, 2.67 mmol) in THF (30 mL) was placed in 50 mL flask, which was flushed with N_2 and the solution was cooled to -78 °C using dry ice/acetone. To the cooled solution, tert-BuLi (1.7 M in pentane, 4.7 mL) was added slowly and stirred for another 30 min at -78 °C and trimethyltin chloride (1.81 g, 9.1 mmol) was directly added as a solid. The solution was slowly warmed to room temperature and allowed to stir for overnight. Aqueous sodium carbonate (30 mL) was added slowly to the solution and extracted with methylene chloride (MC) (100 mL). The resultant organic layer was dried over anhydrous $MgSO_4$ and evaporated the solvent to get yellow residue. The residue was recrystallized from ethanol to obtain 3a as yellow solid (1.1 g, 60%). mp 96–98 °C. ^{1}H NMR (300 MH_Z, $CDCl_3$): δ (ppm) 0.38 (t, 18H), 0.96 (m, 12H), 1.43–1.32 (br, 16H), 1.63 (m, 2H), 2.88 (d, 4H), 7.04 (d, 2H), 7.41 (d, 2H), 7.69 ppm (s, 2H). ^{13}C NMR (600 MH_Z, $CDCl_3$): δ (ppm) 11.15, 14.38, 23.24, 26.05, 29.16, 32.73, 37.31, 42.46, 124.81, 127.68, 130.01, 131.51, 137.24, 142.44, 143.22, 143.82, 153.76. Anal. Calcd for $C_{40}H_{58}S_2Se_2Sn_2$: C, 48.12; H, 5.86; S, 6.42; Se, 15.82; Sn, 23.78. Found C, 48.36; H, 6.02.

2.7.3. Synthesis of 4,8-bis(5-hexyldecylselenophen-2-yl)benzo[1,2-b;4,5-b']dithiophene (3a). 3a was synthesized using 2-hexyldecylselenophene (2.5 g, 6.8 mmol), n-BuLi (2.5 M, 2.8 mL), and 4,8-dihydrobenzo[1,2-b:4,5-b′]dithiophene-4,8-dione (0.6 g, 2.7 mmol) with a similar method to that of 2a as a yellow viscous oil (3 g, 50%). ^{1}H NMR (300 MH_Z, $CDCl_3$): δ (ppm) 0.96 (m, 12H), 1.47–1.29 (br, 48H), 1.66 (m, 2H), 2.92 (d, 4H), 7.04 (d, 2H), 7.39 (d, 2H), 7.43 (d, 2H), 7.65 ppm (d, 2H). ^{13}C NMR (300 MH_Z, $CDCl_3$): δ (ppm) δ 14.1, 22.7, 31.9, 29.3, 29.6, 29.9, 27.5, 33.1, 38.2, 49.7, 109.6, 121.6, 127.9, 128.8, 130.9, 135.3, 144.8, 162.2.

2.7.4. Synthesis of 2,6-bis(trimethyltin)-4,8-bis(5-hexyldecylselenophen-2-yl)benzo[1,2-b;4,5-b']dithiophene (3b). 3b was synthesized using 4,8-bis(5-hexyldecylselenophen-2-yl)benzo[1,2-b;4,5-b']dithiophene (2.5 g, 2.7 mmol), tert-BuLi (1.7 M, 4.09 mL), and trimethyltin chloride (1.3 g, 7 mmol) with a similar method to that of 2b as a yellow semi solid (3 g, 48%). ^{1}H NMR (300 MH_Z, $CDCl_3$): δ (ppm) 0.38 (t, 18H), δ 0.96 (m, 12H), 1.47–1.29 (br, 48H), 1.66 (m, 2H), 2.92 (d, 4H), 7.04 (d, 2H), 7.43 (d, 2H), 7.65 ppm (d, 2H). ^{13}C NMR (600 MH_Z, $CDCl_3$): δ (ppm) 14.34, 14.36, 22.91, 26.89, 29.57, 32.11, 32.14, 33.63, 37.68, 41.01, 124.82, 127.68, 129.99, 130.02, 131.50, 137.23, 142.41, 143.23, 143.81, 153.70. Anal. Calcd for $C_{54}H_{86}S_2Se_2Sn_2$: C, 54.29; H, 7.26; S, 5.37; Se, 13.22; Sn, 19.87. Found C, 54. 02; H, 7.08.

2.7.5. Common method of microwave-assisted polymerization by Stille coupling. In a 10 mL microwave tube, BDTSe monomer (0.5 mmol) and the DTBT or DSeBT monomer (0.5 mmol) was added in CB (3 mL). Then argon was purged into reaction mixture for 15 min followed by the addition of $Pd_2(dba)_3$ (2 mole%) and $(o\text{-tolyl})_3P$ (16 mole%). Then, the mixture was heated in a microwave reactor at 120 °C for 15 min. The reaction mixture was slowly cooled to room temperature, precipitated into methanol (MeOH) and filtered. The obtained solid was purified by Soxhlet method using MeOH, hexane, and acetone. The polymer was obtained from CF, which was evaporated and precipitated into MeOH. The polymer was filtered and dried under vacuum. The yield and results of the polymers are given below:

2.7.6. Synthesis of poly[4,8-bis(5-ethylhexylselenophen-2-yl)benzo[1,2-b:4,5-b']dithiophene-alt-5,6-bis(octyloxy)-4,7-di(selenophen-2-yl)benzo[c][1,2,5]-thiadiazole] (P1). ^{1}H NMR (300 MH_Z, $CDCl_3$): δ (ppm) 7.62−7.32 (br, 6H), 7.20−6.85 (br, 4H), 4.25−4.00 (br, 4H), 3.10−2.75 (br, 4H), 2.20−0.55 (m, 60H). M_n = 46000 g/mol; PDI =1.78. Yield: 46%. Anal. Calcd for: C, 58.17; H, 6.10; N, 2.12; Found: C, 57.90; H, 5.99; N, 2.04.

2.7.7. Synthesis of poly[4,8-bis(5-hexyldecylselenophen-2-yl)benzo[1,2-b:4,5-b']dithiophene-alt-5,6-bis(octyloxy)-4,7-di(selenophen-2-yl)benzo[c][1,2,5]-thiadiazole] (P2). ^{1}H NMR (300 MH_Z, $CDCl_3$): δ (ppm) 7.75−7.25 (br, 6H), 7.20−6.95 (br, 4H), 4.25−4.00 (br, 4H), 3.10−2.75 (br, 4H), 2.20−0.55 (m, 84H). M_n = 45000 g/mol; PDI = 1.76. Yield: 43%. Anal. Calcd for: C, 62.16; H, 7.30; N, 1.81; Found: C, 61.96; H, 7.21; N, 1.78.

2.7.8. Synthesis of poly[4,8-bis(5-ethylhexylselenophen-2-yl)benzo[1,2-b:4,5-b']dithiophene-alt-5,6-bis(octyloxy)-4,7-di(thiophen-2-yl)benzo[c][1,2,5]-thiadiazole] (P3). ^{1}H NMR (300 MH_Z, $CDCl_3$): δ (ppm) 7.60−7.25 (br, 6H), 7.10−6.95 (br, 4H), 4.25−4.00 (br, 4H), 3.10−2.75 (br, 4H), 2.20−0.55 (m, 60H). M_n = 59000 g/mol; PDI =1.86. Yield: 38%. Anal. Calcd for: C, 62.62; H, 6.57; N, 2.28; Found: C, 62.45; H, 6.43; N, 2.15.

2.7.9. Synthesis of poly[4,8-bis(5-hexyldecylselenophen-2-yl)benzo[1,2-b:4,5-b']dithiophene-alt-5,6-bis(octyloxy)-4,7-di(thiophen-2-yl)benzo[c][1,2,5]-thiadiazole] (P4). ^{1}H NMR (300 MH_Z, $CDCl_3$): δ (ppm) 7.70−7.25 (br, 6H), 7.15−6.90 (br, 4H), 4.25−4.00 (br, 4H), 3.10−2.75 (br, 4H), 2.20−0.55 (m, 84H). M_n = 51000 g/mol; PDI =1.80. Yield: 52%. Anal. Calcd for: C, 66.17; H, 7.77; N, 1.93; Found: C, 65.94; H, 7.56; N, 1.85.

3. Results and discussion

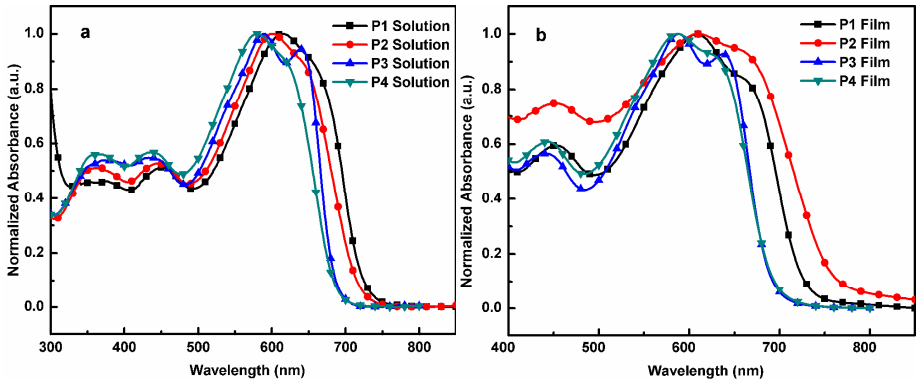

Fig. 1 Normalized UV-visible absorption spectra of polymers in (a) CF solution, (b) thin films.

3.1. Synthesis and characterization

The synthetic routes of monomers and four polymers are shown in Scheme 1. Under nitrogen atmosphere, 1a or 1b was reacted with n-butyllithium followed by the addition of 4,8-dihydrobenzo[1,2-b:4,5-b′]dithiophene-4,8-dione (BDT) to form the corresponding intermediates 2a and 2b as yellow viscous oil. 2a and 2b were finally distannylated by adding tert-butyllithium and trimethyltin chloride to afford monomers 3a and 3b as a yellow solid and semi-solid in reasonable yield of 60 and 48%, respectively. Accordingly, four LBG π-conjugated polymers, **P1-P4** were synthesized by Stille coupling reaction. The final distannylated products (3a, 3b) and **P1-P4** were characterized by ^{1}H, ^{13}C NMR spectroscopy (Fig. S1-S6) and elemental analysis. We make use of the microwave-assisted Stille polymerization method to achieve high molecular weight for the resulting polymers. It was proven that the molecular weight of the polymers can be increased through microwave conditions.[15] All polymerization reactions were conducted using $Pd_2(dba)_3$ as a catalyst and (o-tolyl)$_3$P as a corresponding ligand. **P1-P4** were readily soluble in organic solvents like chloroform (CF), tetrahydrofuran (THF), *o*-dichlorobenzene (ODCB), and chlorobenzene (CB) and the polymerization results are summarized in Table S1. Thermal gravimetric analysis (TGA) was performed to estimate the thermal stability of **P1-P4** and the results are listed in Table S1. **P1-P4** possesses better thermal stability with 5% weight loss showing their decomposition temperatures (T_d) above 300 ^{o}C (Fig. S7).

3.2. Optical properties

The normalized UV-visible absorption spectra of **P1-P4** were measured in CF solution and thin film as shown in Fig. 1a and 1b, respectively. All polymers unveil relatively broad absorption bands, which indicate a significant part of solar flux is absorbed, contributing to photocurrent generation. **P1-P4** showed two distinct absorption bands, which are characteristic for LBG polymers. The absorption band in the longer wavelength corresponds to intramolecular charge transfer (ICT) between BDTSe and BT units and the shorter wavelength band represents π-π* transition of the polymer backbone. The optical bandgap of **P1**, **P2**, **P3**, and **P4** were estimated from the onset absorption edge of thin film absorption spectrum and were found to be 1.69, 1.63, 1.76, and 1.76 eV, respectively as shown in Table 1. It is clearly manifested that the bandgap energy of the polymers (**P1** and **P2**) with selenophene repeating entities are lesser than that of thiophene counterparts (**P3** and **P4**). The thin film ICT absorption onset of selenophene bridged polymers (**P1** and **P2**) is considerably red-shifted when compared to the thiophene counterparts (**P3** and **P4**). This particular interesting feature divulge that the substitution of thiophene with selenophene as a π-spacer group reduces the bandgap owing to enhanced quinoid nature in the polymer backbone.[16] Interestingly, the absorption spectra of **P3** in both solution and film state showed enhanced shoulder peak in the longer wavelength regions, indicating that more planar and ordered structure, also strong interchain π-π stacking and intermolecular packing is present as compared to the other three polymers (**P1**, **P2**, and **P4**). The more planar structure of **P3** is attributed to the non-covalent interactions that exist between the sulfur atom of thiophene π-spacer and oxygen atom of the dialkoxy group on the BT unit. Even though **P4** has exactly similar structure to **P3**, the **P4** shows less pronounced shoulder peak, which might be due to the perturbation created by the sterically hindered lengthy hexyldecyl side chain compared to the ethylhexyl group on the polymer backbone

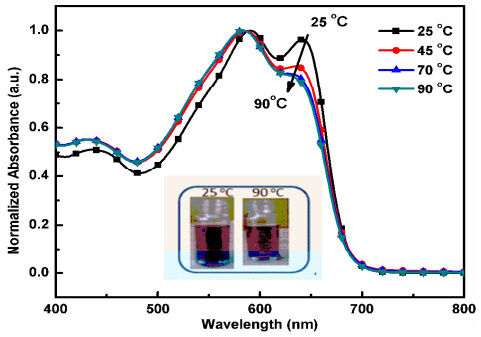

Fig. 2 UV-visible absorption spectra of **P3** in CB (1x10^{-5} M) at 25, 45, 75, and 90 ^{o}C (the inset shows the pictures of the solutions at 25 and 90 ^{o}C).

ultimately, it can be expected that **P3** will exhibit higher hole mobility than the rest of the polymers. It is quite interesting to notice that, **P2** shows a very broad ICT band in film state than their counterparts, indicates that the longer hexyldecyl chain is more favourable for efficient ICT interactions. Due to the strong withdrawing capacity of BT, the four polymers show decent LBGs, which is a key criterion to use them for photovoltaic application. From the absorption profile of **P1-P4**, we can affirmatively state that the π-spacer and alkyl side chain plays a substantial role in influencing the absorption profile of the polymers.

In order to prove the existence of strong aggregation between the polymer chains in **P3**, we conducted variable temperature UV-visible absorption spectra experiments at four different temperatures including 25, 45, 70, and 90 ^{o}C, respectively.

Table 2 Photovoltaic properties of BHJ PSCs of **P1-P4** with or without DIO.

Polymer	Ratio (w/w)	DIO (1 vol%)	V_{oc} (V)	J_{sc} (mA/cm^2)	Integrated J_{sc} (mA/cm^2)	FF (%)	PCE (%)
P1	1:2	no	0.66	9.04	8.02	42.99	2.56
P1	1:2	yes	0.70	12.28	12.14	58.90	5.07
P2	1:2	no	0.71	7.36	7.19	43.15	2.27
P2	1:2	yes	0.73	12.22	12.20	59.35	5.34
P3	1:1	no	0.71	10.93	10.29	52.66	4.09
P3	1:1	yes	0.69	11.75	11.12	53.24	4.16
P4	1:1	no	0.72	7.95	7.78	51.16	2.92
P4	1:1	yes	0.71	10.38	10.26	57.82	4.30

The clear change in the color of **P3** in CB solution was observed at different temperatures and is shown in Fig. 2. Going from 25 to 90 °C, the intensity of the shoulder peak A at 641 nm decreased constantly and the other peak B at 590 nm progressively shifted towards lower wavelength region. These captivating results validate that the pronounced aggregation of **P3** formed in the room temperature solution is disturbed by heating process, which will lead to highly twisted and reduced planar structure for the polymer chains. Due to the strong interchain aggregation tendency for **P3**, it is expected that it would have better charge transport properties compared to other polymers.

3.3. Electrochemical properties

CV was employed to estimate the energy levels of **P1-P4**, the corresponding cyclic voltammograms are shown in Fig. S8 and the data are extracted in Table 1. The HOMO energy levels were calculated to be -5.26, -5.40, -5.20, and -5.22 eV from their onset oxidation potentials. All the polymers possess quite deeper HOMO energy levels, which are necessary for higher V_{oc}, because the V_{oc} is governed by the difference between the HOMO of the donor and lowest occupied molecular orbital (LUMO) of the acceptor. The LUMO energy levels for **P1, P2, P3**, and **P4** were found to be -3.57, -3.77, -3.44, and -3.46 eV, respectively. The LUMO values are reasonably higher than the LUMO energy level of $PC_{71}BM$; this range is quite agreeable for efficient exciton dissociation from the polymers to $PC_{71}BM$ with less charge recombination rate. The incorporation of selenophene ring on BDT resulted in reasonable quite deeper HOMO levels for good air stability. Here, we observed that the alkyl side chains tethered to the π-conjugated backbone have less impact on the electronic energy levels.

3.4. Computational study

Density functional theory (DFT) calculations were performed with Becke's three parameterized Lee−Yang−Parr (B3LYP) exchange functional and 6-311+G(d,p) basis sets except selenium atom for which the LANL2DZ effective core potentials was used. All the calculations were carried out using a suite of Gaussian 09 programs.[17] The HOMOs and the LUMOs of all polymer repeating units were shown in Fig. S9. The orbital distributions clearly show the ICT between each donor and acceptor group. The calculated HOMO energy levels of **P1-P4** were calculated to be –5.13, –5.09, –5.12 and –5.14 eV, respectively, which are in good agreement with the experiment. The HOMO-LUMO energy gaps of **P1-P4** were calculated to be 2.388, 2.396, 2.434, and 2.445 eV, respectively, which are higher than the experiment, however, the tendency is consistent. In particular, the band gaps in selenophene bridged monomers **P1** and **P2** are smaller than those in thiophene bridged monomers **P3** and **P4** due to enhanced quinoid nature in selenophene bridged systems as previously reported. The reason for the overestimation of HOMO-LUMO energy gap in our calculation is that polymer repeating unit geometries were used to compare the polymer systems due to the computational cost.

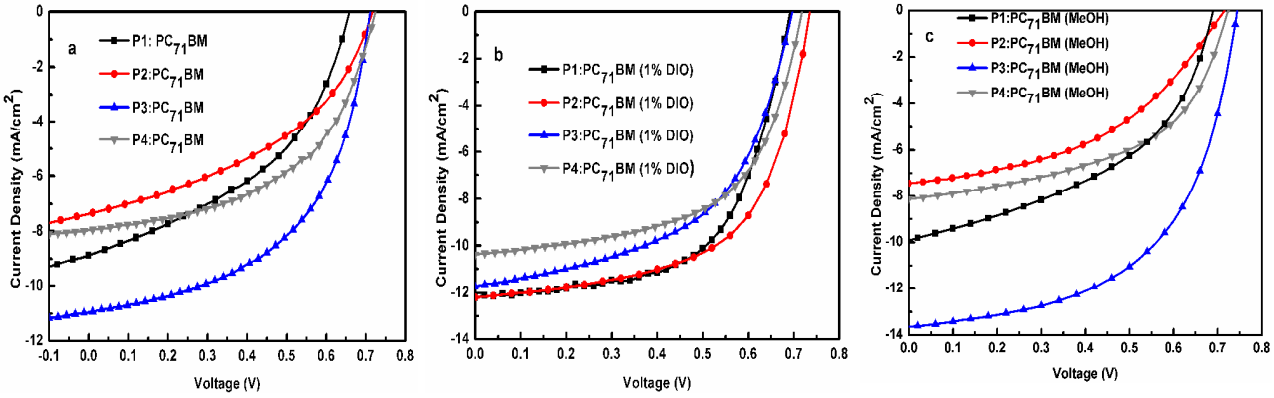

Fig. 3 Current density voltage characteristics of BHJ PSCs of **P1-P4** (a) pristine (b) 1 vol% DIO and (c) methanol treatment.

Table 3 Photovoltaic properties of BHJ PSCs of **P1**-**P4** with methanol treatment.

Polymer	Ratio (w/w)	V_{oc} (V)	J_{sc} (mA/cm^2)	Integrated J_{sc} (mA/cm^2)	FF (%)	PCE (%)
P1	1:2	0.69	9.90	9.40	45.72	3.12
P2	1:2	0.71	7.44	7.32	44.30	2.35
P3	1:1	0.74	13.64	12.31	55.62	5.63
P4	1:1	0.72	8.12	8.11	51.55	3.01

3.5. Organic thin film transistors

The field effect hole mobility (μ_{hole}) of thin films of **P1**-**P4** were measured by fabricating organic thin film transistors (OTFTs). The OTFTs were fabricated on a silicon wafer using bottom contact geometry with channel length (12 μm) and width (120 μm) under N_2 atmosphere. Fig. S10 shows the transfer characteristics of the devices fabricated using the polymers as the active layer, which were annealed at 140 ^oC and the related data is mentioned in Table S2. The polymers should have high charge carrier mobility, as it is very important for achieving better device performance. The OTFTs fabricated with the new polymers as a photoactive layer proved to have p-type transistor characteristics. The OTFTs fabricated using **P1**, **P2**, **P3**, and **P4** exhibited hole mobility (μ_{hole}) of 5.5 x 10^{-3}, 2.3 x 10^{-3}, 7.3 x 10^{-3}, and 3.1 x 10^{-4} $cm^2V^{-1}s^{-1}$, respectively. The **P3** thin film showed highest μ_{hole} among the four polymers, which can be attributed to strong polymer chain packing and enhanced planarity attained by the interaction between the sulfur atom in thiophene π-spacer and the oxygen atom of the dialkoxy group in BT. The mobility data clearly show that the polymers with shorter ethylhexyl side chain (**P1** and **P3**) possess high μ_{hole}, as compared to the polymers with longer hexyldecyl side chain (**P2** and **P4**) (for the fixed alkyl chains on the electron deficient DTBT or DSeBT unit). The lengthy 2-hexyldecyl groups on the BDTSe unit may increase the steric hindrance and make the polymers difficult to pack efficiently, which is very crucial in transporting the holes inside the polymer films. The lowest crystallinity of **P4** was confirmed by x-ray diffraction pattern of the polymer films (shown in the Fig. S11). This is also consistent with the photovoltaic performance of the tested devices (without 1 vol% DIO). It is worth stating that the μ_{hole} values of these polymers are close or above the suggested value (10^{-3} $cm^2V^{-1}s^{-1}$). This means that the loss of photocurrent is reduced and thus high performance will be expected for the OPV devices.[18]

3.6. Photovoltaic characteristics

We fabricated OPV devices to demonstrate the strength of our newly designed polymers as donor materials in BHJ device architecture using $PC_{71}BM$ as an acceptor and the effects of π-spacers and alkyl side chains were investigated. The device structure employed is ITO/PEDOT:PSS/polymer:$PC_{71}BM$/LiF/Al and the photovoltaic performances were measured under the illumination of AM 1.5 G at 100 mW/cm^2. The photovoltaic performances of the OPV devices were tested under various conditions. The CB was used as a processing solvent, the devices fabricated using **P1** and **P2** displayed high J_{sc} and PCE at the ratio of 1:2, whereas the devices based on **P3** and **P4** shown high J_{sc} and PCE at the composite ratio of 1:1. Fig. 3a, 3b, and 3c shows the current density-voltage (*J*-*V*) characteristics of the BHJ PSCs of pristine, 1 vol% of DIO, and methanol treatment. The photovoltaic parameters of devices obtained from the best optimized conditions are summarized in Table 2 and 3. The optimum thickness of the BHJ thin films was found to be approximately in the range of 85~90 nm for **P1**, **P3** and 95~100 nm for **P2**, **P4** respectively. The device based on the **P1**:$PC_{71}BM$ (1:2 wt%) blend exhibited a V_{oc} of 0.66 V, a J_{sc} of 9.04 mA/cm^2, an fill factor (FF) of 42.99% with a reasonable PCE of 2.56% and the device based on the **P2**:$PC_{71}BM$ (1:2 wt%) blend demonstrated a V_{oc} of 0.71 V, a J_{sc} of 7.36 mA/cm^2, an FF of 43.15% with PCE of 2.27%. However, the device based on the **P3**:$PC_{71}BM$ (1:1 wt%) blend exhibited a V_{oc} of 0.71 V, a J_{sc} of 10.93 mA/cm^2, an FF of 52.66% with a moderate PCE of 4.09% and the device based on the **P4**:$PC_{71}BM$ (1:1 wt%) blend demonstrated a V_{oc} of 0.72 V, a J_{sc} of 7.95 mA/cm^2, FF of 51.16% with PCE of 2.92%.

Interestingly, in pristine devices based on **P3**:$PC_{71}BM$ shown the highest J_{sc} followed by greater PCE. Another intriguing result that need to be addressed is the FF for the device based on **P3**:$PC_{71}BM$ (1:1 wt%). **P3**-based device exhibited high FF of 52.66% when compared to the devices based on the other three polymers. This could be due to the high μ_{hole} of 7.3 x 10^{-3} $cm^2V^{-1}s^{-1}$ obtained from the OTFT results.

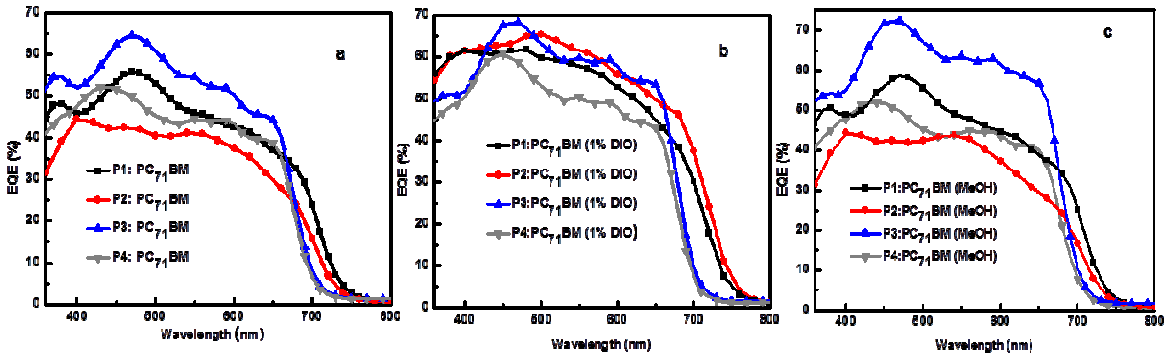

Fig. 4 EQE spectra of the BHJ PSCs of **P1**-**P4** (a) without additive, (b) with 1 vol% DIO, and (c) methanol treatment.

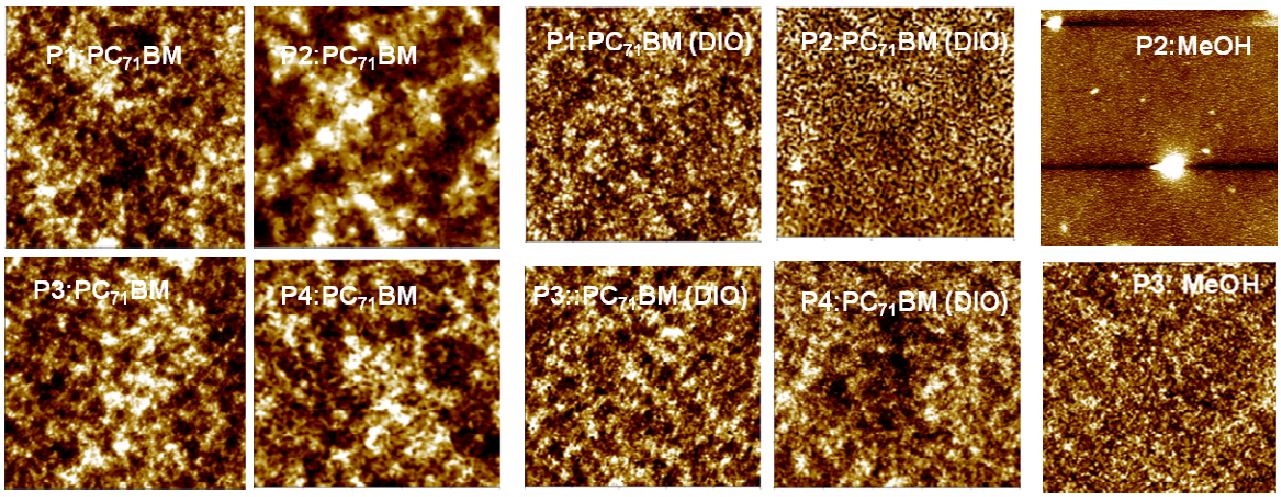

Fig. 5 AFM images of active layers (pristine, DIO, and MeOH) of **P1-P4.**

When pristine CB was used as a processing solvent for the device fabrication, **P3** and **P4**-based devices (thiophene as a π-spacer) dominated the **P1** and **P2**-based devices (selenophene as a π-spacer) in terms of PCE. We ascribe this phenomenon to the higher FF values of the **P3** and **P4**-based devices. The OPV devices with hexyldecyl side chain exhibited low PCE, when compared to the devices with ethylhexyl side chain. We assume that too lengthy and bulkiness of the side chains reduce the miscibility of polymer with $PC_{71}BM$, leading to excessive phase separation between polymer chains and $PC_{71}BM$ molecules and thereby reducing the interfacial areas for charge separation in **P2** and **P4**-based solar cells. The related smaller currents lead to the diminished OPV performances in the case of **P2** or **P4.** The 2-hexyldecyl side chains weakened the intermolecular interactions thus leading to low J_{sc} for **P2** and **P4**-based devices, whereas the 2-ethylhexyl group preserved the interactions, concomitantly gave better J_{sc} for **P1** and **P3**. Particularly, **P3** shows decent PCE of 4.09% for the pristine blend film due to higher J_{sc}, FF, and V_{oc} than that of its counterparts. This can be comprehended by planar backbone of **P3** that drives to form better interpenetrating network in the active layer. The FF values of thiophene bridged polymers (**P3**, **P4**) are higher than that of selenophene bridged polymers (**P1**, **P2**). This phenomenon indicates that more charge trapped sites are present in selenophene bridged polymers, which hampers the charge collection at the corresponding electrodes.

There have been reports that the FF and J_{sc} of OPV devices could be greatly improved by using additives such as DIO and CN by forming excellent morphology of the active layer. To further improve the photovoltaic performance of **P1**, **P2**, **P3**, and **P4**, an optimal amount of DIO (1 vol%) was introduced. These high boiling additives can adjust the morphology to attain nanoscale phase separation of the polymer:$PC_{71}BM$ blends during spin coating and consequently significant improvement in PCE could be visualized. Surprisingly, interesting observations were recognised after introducing optimum amount (1 vol%) of DIO. We observed PCE of 5.07, 5.34, 4.16, and 4.30% for the devices of **P1**, **P2**, **P3**, and **P4** respectively. The most efficient **P2**-based device, obtained using 1% DIO, had an average PCE of. 5.34%, with J_{sc} of 12.22 mA/cm^2, FF of 59.35%, and V_{oc} of 0.73 V. The effect of DIO is much strongly pronounced in the case of devices based on **P1** and **P2**, when compared to the **P3** and **P4**. However, the overall PCE was increased for all the devices based on **P1**, **P2**, **P3,** and **P4** after adding 1% DIO. The change of PCE is primarily due to the improved FF and J_{sc}. **P1** and **P2**-based devices displayed significantly increased J_{sc} and FF (shown in Table 2) leading to higher device performances. We presume that DIO facilitated the polymer:$PC_{71}BM$ phase separation and increase intermolecular packing to realize high PCE for the OPV devices. After adding DIO, the establishment of appropriate phase separation in the films of **P3** and **P4**-based devices is less effective than that of **P1** and **P2**, which could be the reason for less improved efficiency. We tested the OPV performance of BHJ PSCs by adding more than 1% DIO, but we did not observe any promising results. We also tested BHJ PSCs with CN as additional additive and obtained moderately high PCE; the photovoltaic properties of **P1-P4** were improved than their neat blends except in **P3**, and the resulting photovoltaic properties are displayed in Table S3.

It is well proven that the nanoscale phase separation of the thin film active layer of PSC will be occurred; when the methanol treatment method is applied in BHJ PSCs.[19] Here we also tried to employ methanol treatment to further optimize photovoltaic properties of **P1-P4** based PSCs. The general process of methanol treatment involves few steps like spin coating the active layers followed by addition of small amount of methanol on top of it and wait for few seconds and spinning the device at high rpm to spin off the methanol. To our surprise, after methanol treatment on **P1-P4** based devices, **P3** showed much improved photovoltaic performance than the other polymer blends.

Table 4 Results of Mott-Schottky analysis of the **P3**:$PC_{71}BM$ BHJ PSCs with and without methanol treatment.

Solvent treatment	V_{oc} (V)	N (cm^{-3})	V_{bi} (V)	w (nm)
P3 (none)	0.71	3.91 x 10^{16}	0.77	88
P3 (MeOH)	0.74	6.11 x 10^{16}	0.80	72

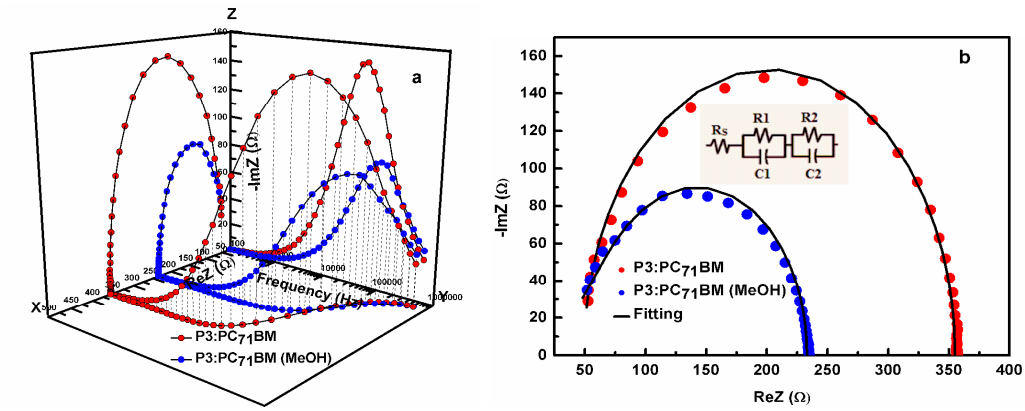

Fig. 6 (a) 3D perspective plot of **P3**:$PC_{71}BM$ devices without and with methanol treatment showing impedance response, (b) Nyquist plot of **P3**:$PC_{71}BM$ devices without and with methanol treatment (the insets shows the equivalent circuit).

The PCE of **P3** raised from 4.09 to 5.63% with an enhanced J_{sc} (13.64 from 10.93 mA/cm^2) and FF (55.62% from 52.66%). This enhanced photovoltaic properties of **P3** based PSCs is because of methanol much effectively fine tuned the active layer morphology of **P3** than others. Consequently, the charge mobility will be increased due to the excellent BHJ interface for charge dissociation and collection, thus delivering a high J_{sc}, FF, and PCE for the corresponding PSC device. We assume that enhanced backbone planarity of **P3** could be the reason for easy migration of $PC_{71}BM$ molecules after methanol treatment. The enhancement of photovoltaic performance due to the effect of methanol treatment **P3** was further analyzed deeply by electrical impedance spectroscopy and SCLC mobility study.

Fig. 4a, 4b, and 4c shows the external quantum efficiency (EQE) curves of the devices based on polymer:$PC_{71}BM$ without and with 1 vol% DIO and methanol treated devices. As shown in Fig. 4, the EQE curves of the devices show that the OPV devices have good response to the sunlight over the range from 350 to 750 nm. The shapes of the EQE curves of the devices based on polymer:$PC_{71}BM$ are similar to their absorption spectra. This indicates that major amount of the absorbed photons of the polymers contribute to the photocurrent generation. The EQE plots of the devices with DIO showed much higher photovoltaic response than those without DIO. This may be due to the establishment of the improved morphology by efficient intermixing of polymer donor and fullerene acceptor than their pristine counterparts. And also methanol treated devices also showed enhanced EQE spectra than their pristine counter parts. Particularly, **P3** based PSCs showed much enhanced EQE spectrum after methanol treatment which well correlated with the enhanced J_{sc}. The J_{sc} values calculated from integration of the EQE spectra concur well with J_{sc} obtained from the *J–V* measurements.

3.7. Morphology

The morphology of the photoactive layer plays an important role in the photovoltaic performance of PSCs along with other photo-physical properties and in several situations the performance of the device strongly depends on its morphological features. To gain more understanding on the effect of the additive and alkyl side chains on the morphology of the **P1-P4** blend films, atomic force microscopy (AFM) images of active layers of the optimized devices with and without DIO were taken and the corresponding AFM images are shown in Fig. 5. We encountered different morphological scenarios upon addition of 1 vol% DIO to the four polymer blends at their optimized ratios, After adding DIO, a well-developed morphology and better interpenetrating network of **P1**:$PC_{71}BM$, **P2:**$PC_{71}BM$, and **P4:**$PC_{71}BM$ is accomplished, as compared to **P3**:$PC_{71}BM$ which is highly beneficial to the charge transport. The DIO, which is added to the active layer, encouraged to form more specific and aggregated donor polymer domains. Ultimately, a favourable charge separated state will occur in the BHJ network, this will give good support to the movement of the free charges to the corresponding electrodes. The excellent percolation path for the movement of free charges is clearly evidenced by the increased FF and J_{sc} values after addition of DIO. Overall the suitable morphology of the blend films are consistent with the higher photovoltaic performance of the PSCs based on **P1, P2, P3,** and **P4**. AFM studies were carried out for the methanol treated active layers to understand the surface morphology after methanol treatment, a common phenomenon observed among all active layers, i.e. root mean square (RMS) roughness slightly increased due to $PC_{71}BM$ aggregation and in case of **P3** mixing was much homogeneously occurred as shown in Fig. 5.

X-ray diffraction technique was used to test the crystalline properties of polymer thin films, and XRD patterns are shown in Fig. S11. From the data, it was observed that **P1-P4** thin films are found to be low crystalline in nature. Further, **P4** shows very weak crystallinity among four polymers, which was agreed with low hole mobility of **P4**.

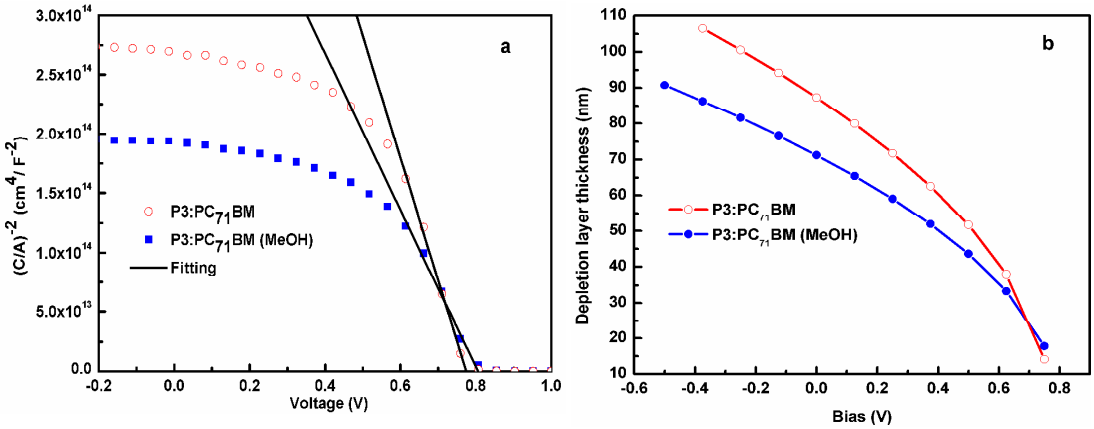

Fig. 7 (a) Mott-Schottky analysis of the **P3**:$PC_{71}BM$, (b) depletion layer thickness of **P3**:$PC_{71}BM$ devices without and with methanol treatment over bias voltage.

3.8. Impedance spectroscopy studies

The enhancement of photovoltaic performance due to the effect of methanol treatment in **P3** was analyzed using impedance spectroscopy.[20,21] Fig. 6a displays the 3D perspective plot depicting dependence of real and imaginary part of impedance on the frequency, the real and imaginary part of the impedance is resistance and reactance respectively. The X-Y, Y-Z and X-Z plane in the 3D plot shows the resistance vs frequency, the reactance vs frequency characteristics and the Nyquist plot respectively. The Nyquist plots of impedance measurement of **P3**:$PC_{71}BM$ device along with the corresponding equivalent circuit (EC) is shown in Fig. 6b in both pristine and methanol treated conditions. These plots were substantially consistent with fitting curve simulated by an EC. The R_s corresponds to series resistance consisting of ohmic components. The R1 and C1 corresponds to bulk resistance and capacitance, whereas the R2 and C2 correspond to depletion layer functioning. The methanol treated device has a significantly reduced bulk resistance as indicated by the decreased radius in the Nyquist plot. The bulk resistance can be obtained from the diameter of the semicircle on the "ReZ" axis. This result indicates that the methanol treatment reduced the interface resistance between the active layer and cathode, leading to a lower device resistance. In addition, the intercept on "ReZ" axis at high frequencies in Nyquist plots gives the series resistance. Following methanol treatment, R_s is reduced from 4.48 to 3.12 Ω cm^2 for **P3.** This agrees with the observed increase in J_{sc} and FF. A semiconductor has a charge carrier concentration (N), which effects the distribution of the electric fields within the device. If the carrier concentration is within a certain range, then a Schottky contact is formed at a metal-semiconductor interface and a built-in potential (V_{bi}) is present. To estimate V_{bi}, the C-V characteristics were examined using the following Mott-Schottky equation, $C^{-2} = 2(V_{bi} - V)/A^2e\varepsilon_r\varepsilon_0N$. Here, V, e, ε_r, ε_0, N, A, and C, respectively, denote the bias voltage, charge, relative dielectric constant (ε_r=3), permittivity in vacuum, charge carrier concentration, device active area, and capacitance for each bias voltage. The linear region under low forward bias is related to the formation of a Schottky contact and can be fitted to a plot of C^{-2} versus bias voltage. V_{bi} can be evaluated by extrapolation of C^{-2}=0, whereas the slope of the line gives the charge carrier concentration with equation, $N=-2/slope.A^2e\varepsilon_r\varepsilon_0$ derived from the Mott-Schottky equation. The methanol treated device shows higher V_{bi} and pronounced increase in N as shown in Fig. 7a. The V_{bi}, which plays key role in the internal electric field in BHJ PSCs, is an important parameter and gives the upper limit for V_{oc}. The V_{bi} also considered to be responsible for excitons dissociation.[22] Thus, the increase in V_{bi} may be responsible for the increase in V_{oc} in the devices with methanol treatment. The higher order of N in case of methanol treated device showed enhanced surface charge density. Important aspect resulting from the Mott-Schottky analysis is the depletion zone width (w) at zero applied bias, $w=(2\varepsilon(V_{bi}-V)/eN)^{1/2}$.

In the dark at negative bias as shown in Fig. 7b, the depletion layer gets bigger than the thickness of the device, and the capacitance should not change anymore. It is clearly manifested in Table 4, the depletion width practically reaches the anode for the methanol untreated devices, whereas it is comparatively reduced for methanol treated devices and pictorially represented in Fig. 8. The intrinsic p-doped nature of semiconducting polymer leads the formation of Schottky contact upon deposition of metal electrode onto the active layer of the BHJ. E_F is the fermi level of the p-type semiconducting polymer which is lower than fermi level of the metal in a Schottky diode as shown in Fig 8a, where ϕ_m is the work function of the metal electrode. If there is a contact between the metal and the semiconductor, respective charges will move across the interfaces to provide an equilibrium uniform Fermi level as shown in Fig 8b and 8c. In semiconductor region close to the metal contact are no mobile charges anymore and this region called depletion layer and has width w. For connected system in the dark, the depletion width (w = 88 nm) reaches the anode (active layer thickness) for pristine device (Fig. 8b), whereas it is reduced (w= 72 nm) for MeOH treated devices (Fig. 8c). This is mainly because of the difference in doping between the pristine and methanol treated device. The higher doped layers confine the electrical field in the vicinity of the cathode, allowing extraction of V_{bi} and N.[23, 24]

We observed dramatic increase in the J_{sc} and FF of the PSCs after methanol treatment method. To understand this SCLC model was employed to investigate the charge transport properties. The hole and electron mobilities of **P3** based devices were improved after methanol treatment 3.62 x 10^{-4} and 2.36 x 10^{-4} $cm^2V^{-1}s^{-1}$ from 2.16 x 10^{-4}, 1.61 x 10^{-4} $cm^2V^{-1}s^{-1}$ respectively, which are well correlated with increased J_{sc} and FF. It is concluded that increased carrier mobility of BHJ PSCs of **P3** after methanol treatment results high J_{sc} and FF thus results high PCE.

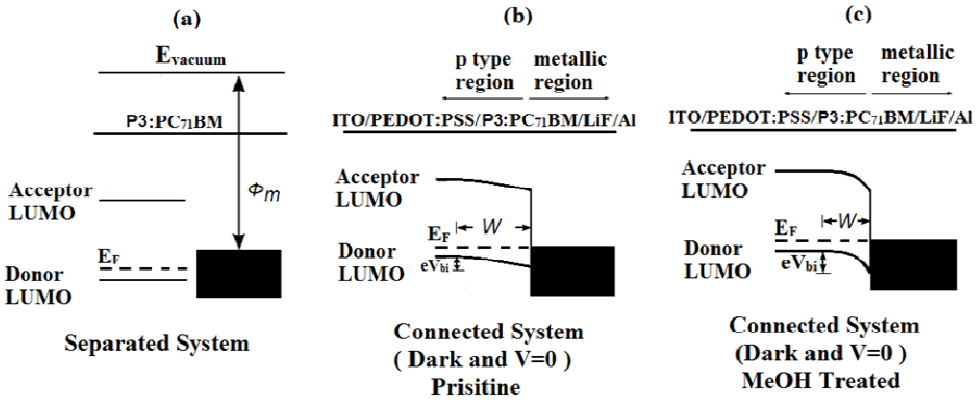

Fig. 8 Energy band diagram of a p-type Schottky contact along with depletion layer thickness w for connected system. (a) Metal and p-doped donor polymer (**P3**): acceptor (fullerene) in separated system (b) connected system for pristine devices, and (c) connected system for methanol treated devices.

4. Conclusions

In summary, we have studied systematically how the alkyl side chain variation and the different π-spacer groups affect the optical, charge carrier, and photovoltaic properties of BDTSe-based π-conjugated polymers. The existence of both non-covalent interactions between sulfur atom in thiophene and oxygen atom in dialkoxyBT and shorter ethylhexyl side chain in **P3** makes it highly planar backbone structure among the four polymers. When shorter ethylhexyl side chains are replaced with longer hexyldecyl side chains, it resulted in significant effect on the hole mobility of the polymers. This illustrates that the alkyl side chain substituents can significantly impact the polymer packing for better charge transport. The device fabrication results revealed that by modulating the processing conditions via usage of external additive like DIO during device fabrication, the proper rearrangement of BHJ network happens in such a way to attain higher PCE. Consequently, when **P1**, **P2**, **P3**, and **P4** were blended with $PC_{71}BM$ in BHJ fashion, PCE of 5.07%, 5.34%, 4.16%, and 4.30% were accomplished for the devices based on **P1**, **P2**, **P3**, and **P4** respectively. In addition, methanol treatment also showed improved PCE for **P1-P4** and delivered a high PCE of 5.63% for **P3**. On the account of the intriguing results that have been perceived, we conclude about the design of our current research work: 1) the disparity in the size of alkyl side chain is very important parameter for designing efficient PSCs materials, as they can significantly impact charge transport; 2) the nature of π-spacer inserted between the electron rich and electron deficient units to influence the planarity of polymer backbone; 3) implementing proper device fabrication conditions like usage of external additives or polar solvent exposure like methanol to improve the miscibility of the polymer with $PC_{71}BM$ to obtain well organized interpenetrating network to realize high PCE. Having potential applications for PSCs, investigation into further augmenting the PCE of these polymers is underway.

Acknowledgments

This work was supported by grant fund from the National Research Foundation (NRF) (2011-0028320) and the Pioneer Research Center Program through the NRF (2013M3C1A3065522) by the Ministry of Science, ICT & Future Planning (MSIP) of Korea.

Notes and references

[a] *Department of Chemistry Education, Graduate Department of Chemical Materials, BK 21 PLUS Team for Advanced Chemical Materials, and Institute for Plastic Information and Energy Materials, Pusan National University, Busan, 609-735, Republic of Korea. E-mail addresses: shjin@pusan.ac.kr (S.-H. Jin), Tel.: +82 51 510 2727; fax: +82 51 581 2348*
[b] *Department of Chemistry, Sungkyunkwan University, Suwon 440-746, Republic of Korea*
[c] *Department of Chemistry, The Catholic University of Korea, Bucheon 420-743, Republic of Korea*
[d] *Surface Technology Division, Korea Institute of Material Science, Changwon 641-83, Republic of Korea*
[e] *Advanced Analysis Center, Korea Institute of Science and Technology (KIST), Seoul 136-791, Republic of Korea*
[f] *Photo-electronic Hybrids Research Center, Korea Institute of Science and Technology (KIST), Seoul 136-791, Republic of Korea*

‡ These authors contributed equally to this manuscript
† Electronic Supplementary Information (ESI) available: See DOI: 10.1039/b000000x/

1 S. Gunes, H. Neugebauer, N.S. Sariciftci, *Chem. Rev.*, 2007, **107**, 1324-1338.
2 G. Yu, J. Gao, J.C. Hummelen, F. Wudl, A.J. Heeger, *Science*, 1995, **270**, 1789-1791.
3 J. You, L. Dou, K. Yoshimura, T. Kato, K. Ohya, T. Moriarty, K. Emery, C.-C. Chen, J. Gao, G. Li, Y. Yang, *Nat. Commun.*, 2013, **4**, 1446.
4 H.-Y. Chen, J. Hou, S. Zhang, Y. Liang, G. Yang, Y. Yang, L. Yu, Y. Wu, G. Li, *Nat. Photon*., 2009, **3**, 649-653.
5 J. Peet, J.Y. Kim, N.E. Coates, W.L. Ma, D. Moses, A.J. Heeger, G.C. Bazan, *Nat. Mater*., 2007, **6**, 497-500.

6 Y. Kim, S. Cook, S.M. Tuladhar, S.A. Choulis, J. Nelson, J.R. Durrant, D.D.C. Bradley, M. Giles, I. McCulloch, C.-S. Ha, M. Ree, *Nat. Mater.,* 2006, **5**, 197-203.

7 M. Zhang, X. Guo, Z.-G. Zhang, Y. Li, *Polymer*, 2011, **52**, 5464-5470.

8 L. Huo, J. Hou, S. Zhang, H.-Y. Chen, Y. Yang, *Angew. Chem*., Int. Ed., 2010, **49**, 1500-1503.

9 (a) M. Heeney, W. Zhang, D.J. Crouch, M.L. Chabinyc, S. Gordevev, R. Hamilton, S.J. Higgins, I. McCulloch, P.J. Skabara, D. Sparrowe, S. Tierney, *Chem. Commun*. 2007, 5061-5063. (b) Y. Li, *Acc. Chem. Res*., 2012, **45**, 723-733**.** (c) C. Cui, W.-Y. Wong, Y. Li, Energy Environ. Sci., 2014, 7, 2276-2284. (d) S. Zhang, L. Ye, W. Zhao, D. Liu, H. Yao, J. Hou, Macromolecules, 2014, 47, 4653-4659.

10 M.H. Chen, J. Hou, Z. Hong, G. Yang, S. Sista, L.M. Chen, Y. Yang, *Adv. Mater*., 2009, **21**, 4238-4242.

11 P. Shen, H. Bin, L. Xiao, Y. Li, *Macromolecules*, 2013, **46**, 9575-9586. (b) Kranthiraja, K.; Gunasekar, K.; Cho,W.; Song, M.; Park, Y. G.; Lee, J.Y.; Shin, Y.; Kang, I.-N.; Kim, A.; Kim, H.; Kim, B.; Jin, S.-H. *Macromolecules*, **2014**, *47*, 7060-7069.

12 S. Nam, J. Jang, H. Cha, J. Hwang, T.K. An, S. Park, C.E. Park, *J. Mater. Chem*., 2012, 22, 5543-5549.

13 X. Guo, R. P. Oritz, Y. Zheng, M.-G. Kim, S. Zhang, Y. Hu, G. Lu, A. Facchetti, T.J. Marks, *J. Am. Chem. Soc.,* 2011,**133**, 13685-13697.

14 P. Ding, C.-C. Chu, B. Liu, B. Peng, Y. Zou, Y. He, K. Zhou, C.-S. Hsu, *Macromol. Chem. Phys*., 2010, **211**, 2555-25561.

15 R.C. Coffin, J. Peet, J. Rogers, G.C. Bazan, *Nat. Chem*., 2009, **1**, 657-661.

16 S.S. Zade, N. Zamoshchik, M. Bendikov, *Acc. Chem. Res*., 2010, **44**, 14-24.

17 M.J. Frisch, et al. Gaussian 09, Revision A. 1, Gaussian, Inc.; Wallingford CT, 2009.

18 K.M. Coakley, M.D. McGehee, *Chem. Mater*., 2004, **16**, 4533-4542.

19 X, Liu, W. Wen, G.C. Bazan, *Adv. Mater*., 2012, **24**, 4505-4510.

20 Z. Tan, C. Yang, E. Zhou, X. Wang, Y. Li, *Appl. Phys. Lett*.,2007, **91**, 023509.

21 L.W. Leong, S.R. Cowan, A.J. Heeger, *Adv. Energy. Mater.,* 2011, **1**, 517-522.

22 K.M. O'Malley, C.-Z. Li, H.-L. Yip, A.K.-Y. Jen, *Adv. Energy Mater*., 2012, **2**, 82-86.

23 M. Vasilopoulou, D.G. Gerorgiadou, A.M. Douvas, A. Soultati, V. Constantoudis, D. Davazoglou, S. Gardelis, L.C. Palilis, M. Fakis, S. Kennou, T. Lazarides, A.G. Coutsolelos, P. Argitis, *J. Mater. Chem. A.,* 2014, **2**, 182-192.

24 P. P. Boix, J. Ajuria, I. Etxebarria, R. Pacios, G.G. Belmonte, J. Bisquert, *J. Phys. Chem. Lett*., 2011, **2**, 407-411.

Graphical Abstract

5

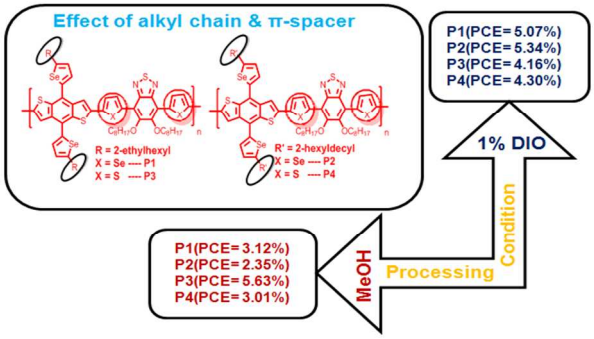

Collective effect of π-spacers, alkyl side chains, and of the various processing conditions on optoelectronic properties of **P1-P4**.